

UDK: 625.074; 546.65; 661.847.532.1

Assessment of Efficiency of Rare Earth Elements Recovery from Lignite Coal Combustion Ash via Five-Stage Extraction

Ljiljana Miličić¹, Anja Terzić^{1*)}, Lato Pezo², Nevenka Mijatović¹, Ilija Brčeski³, Nikola Vukelić⁴

¹Institute for Testing of Materials IMS, Vojvode Mišića Bl. 43, 11000 Belgrade, Serbia

²Institute of General and Physical Chemistry, University of Belgrade, Studentski Trg 12-16, 11000 Belgrade, Serbia

³Faculty of Chemistry, University of Belgrade, Studentski Trg 12-16, 11000 Belgrade, Serbia

⁴Faculty for Physical Chemistry, University of Belgrade, Studentski Trg 12-16, 11000 Belgrade, Serbia

Abstract:

Rare earth elements (REE) are frequently referred to as ingredients for enhancements in modern industry, as they are extensively applied in many industrial branches due to their accentuated electro-magnetic and optical properties. REE have end-utilizations as catalysts, magnets, and as dopants for ceramic materials. Rare earth minerals are scarce therefore the unconventional REE-containing resources such as waste materials and industrial byproducts are continuously being investigated. Coal combustion products comprise REE concentrations varying between 200 ppm and 1500 ppm. This quantity can be isolated through the extraction procedure. In this study, the five stages extraction was conducted on the coal combustion ash from the selected landfill site. The extractions of 32 elements (As, Ga, Ce, Be, Ge, Nd, Cr, Zr, Eu, Cu, Nb, Gd, Co, Mo, Dy, Li, Ag, W, Mn, Cd, Au, Ni, In, Hg, Pb, Sn, Tl, V, Sb, Th, Zn, and La) were conveyed. Chemical analyses were conducted via XRF, ICP-OES, ICP-MS, and AAS techniques. The complexity of the obtained data was examined by Principal component analysis and Cluster analysis in order to derive interconnections between quantity of elements and landfill characteristics, as well as mutual relationships among the elements of interest, and to assess the accomplishment of REE recovery from the coal ash.

Keywords: Powdery materials; Industrial byproduct; Chemical extraction; Analytical modeling; Dopants for ceramic materials.

1. Introduction

The ash generated as a by-product of the coal combustion in power-plants represents a huge ecological and financial peril. According to the information provided by Ecoba, approximately 40 million tons of coal combustion products (CCP) are annually produced in the European Union [1]. Within the EU, the reutilization rate for fly ash in the construction industry is currently at approximately 43 %, for bottom ash around 46 %, and for boiler slag is 100 % [1, 2]. The rest of CCP ordinarily finishes its life-cycle at the waste materials depots.

*) Corresponding author: anja.terzic@institutims.rs

Improperly arranged and maintained landfills are potential source of environmental pollution, which includes soil and ground-water contamination due to the leaching of the toxic matter from CCP [3-8]. Thereby, the management of CCP and revitalizing it from a waste material into useful resource became one of the most important quests in the contemporary scientific researches. The investigations are taking place in multiple fields, since the coal ash can be utilized in cement production [9-12], building composite materials [13-15], ceramics [16, 17], and geotechnical applications [18, 19].

Upon the combustion, the mineralogical composition previously present in the coal remains approximately the same in the produced ash. Generally, the chemical and mineral-phase composition, as well as the proportion of the fly ash in the total amount of the CCP depends on the type of the combustion process and the applied type of fuel [20-22]. The coarse fractions of the CCP are being released at the boiler bottom. The fine fractions, i.e. fly ash, are scooped from electro-filters where they have been taken by combustion exhaust gas. Even though the chemical composition of the coal ash depends on the coal, fuel and the combustion process applied, the majority of the researches came to the mutual agreement that silicon, aluminum, calcium and iron participate as the CCP's predominant chemical elements [23-25]. The carbon content exhibits the highest dependence on the characteristics of the combustion procedure. Analogously, the loss on ignition (LoI) can significantly vary – from 1 % to over 20 % (tolerable value of LoI in the civil engineering industry is 5-9 %). Besides the main elements (Si, Al, Fe, and Ca) usually bonded in the form of oxides, and organic matter, CCP comprises a number of trace elements, i.e. heavy metals and rare earth elements (REE) [26, 27]. These compounds found in traces remain in the ash structure regardless of the classification, milling or beneficiation procedure applied [28-30].

Rare earth elements are a group of seventeen chemical elements that include all lanthanides, and additional - scandium and yttrium. The REE are highly important materials which are utilized in a wide range of either commercial or military applications [31, 32]. Namely, these resources are used in the communications sector, energy production, environmental protection and national security [32, 33]. Due to their accented electro-magnetic and optical properties, REE are the most commonly applied as doping agents in ceramic and composite materials which are then employed in lasers, catalysts, permanent magnets, rechargeable batteries, etc. [33-37]. Since the world's reserves of rare earths are scarce, each of the secondary products that comprise these elements is highly evaluated. Usable presence of REE in the waste materials such is coal ash was first noticed in 1930's by Goldschmidt, and since then a wide specter of combined enrichment and extraction technologies has been applied to the coal based industrial byproducts [32, 38].

Recovery of the valuable REE from the coal combustion ash is an expensive procedure. Extenuating circumstance is that landfilled coal combustion products otherwise would be treated as a waste material and a potential source of pollution. The employment of these byproducts in the recovery of REE provides them with a new market value. Upon identification of the coal combustion products on a landfill site, and subsequent assessment of the material with the highest rare earth elements concentration, the byproducts are submitted to the extraction procedure. The REE extraction is usually conducted in several stages [39-43]. The length and cost of the extraction procedure requires precise planning and assessment of the obtained results in order to determine the cost-effectiveness of each extraction phase. Therefore, chemometric approach has been used in this investigation. Pattern recognition techniques (Principal Component Analysis - PCA and Cluster Analysis - CA) were applied to the experimental data (used as descriptors) to characterize and differentiate among the observed samples. The goal of the investigation was to develop an environmentally benign and economically competitive technology to extract REE from the unconventional resource and thereby secure domestic supply of these critical materials.

2. Materials and Experimental Procedures

The coal combustion ash was obtained from the landfill of TENT-A power-plant in Serbia. The locations of the boreholes were decided upon assessment of the possibilities of access and immediate exploitation. The sampling of the ash was conveyed at different positions on the landfill. Various sampling depths were used. Superficial samples (i.e., ash sampled from the depths less or equal to 50 cm) were unattended due to the heterogeneity caused by atmospheric impact. The samples from the bottom of boreholes were also excluded from the consideration in the experiment, due to the contamination of the coal ash with the soil. The analytical sample was taken from the borehole's core and prepared for the further analyses via standard quartering method. A total of 500 ash samples were obtained from TENT-A landfill. The boreholes positions (x) were: 4, 7, 12, 15, 19, and 22. Depths of the sampling positions (y) for each borehole were: 5, 10, 15, and 19 m. Thereby, the coal ash samples were labeled as Bx-y: B4-5/10,15,19; B7-5/10,15,19; B12-5/10,15,19; B15-5/10,15,19; B19-5/10,15,19; and B22-5/10,15,19 (Fig. 1).



Fig. 1. Positions of the boreholes on the TENT-A landfill (source of the image Google Maps).

2.1 Sequential extraction procedure

Sequential extraction of REE from the coal combustion ash comprised five stages:

Stage 1 (SI): ash samples (100 g) were placed in the glass flasks filled with 900 ml of 1M ammonium acetate solution. The flasks were set on a laboratory rotary mixer. The pH value of the prepared solution was 7. The control testing solution comprised the extraction agent (900 ml). The duration of the extraction procedure was 120 min. Upon conducted extraction the samples were rested for 12 hours in order to achieve better phase separation. The liquid phase was filtrated. The solid residue was leached with water until the negative reaction on ammonium ions was established. The solutions were concentrated up to 400 ml. The procedure was conveyed at temperatures below the boiling point. Afterwards the solutions were poured into a volumetric flask and diluted up to 500 ml. Thus obtained samples were flowed into plastic flasks and hermetically sealed. The residue was returned into the starting glass flask.

Stage 2 (SII): the residue from the SI was diluted with 400 ml of 0.2 M hydroxylamine hydrochloride and 0.02 M hydrochloric acid. The pH value was set at 4 with the use of 0.6 M hydrochloric acid. The control testing solution comprised the extraction agent (800 ml). The extraction was conducted on a rotary mixer during 12 hours with periodical opening of the flasks in order to acquire the atmospheric pressure balance. Upon extraction, the suspensions were immediately filtrated, and the solid residue was leached with water until the negative reaction on ammonium ions was established. Obtained solutions were

concentrated up to 400 ml, diluted to 500 ml and then poured into hermetically sealed plastic flasks. The residue was returned into the starting glass flask.

Stage 3 (SIII): 400 ml of 0.4 M oxalic acid and 0.4 M of ammonium oxalate were added to the suspension from the SII. The control testing solution contained adequately concentrated extraction agent (800 ml). The extraction was conducted manually during the initial 3 hours. Each procedure lasted for 1 min and was repeated at 10 min intervals, with the opening of the flasks for atmospheric pressure balance to be acquired. Afterwards, the extraction was continued on the rotary mixer for another 7 hours. The suspensions were then rested for 12 hours in order to achieve better phase separation. The filtration and residue leaching were conducted in the exactly the same manner as in the previous stages, i.e. until the negative reaction on oxalates was established. The obtained solutions were concentrated up to 400 ml, diluted to 500 ml and poured into hermetically sealed plastic flasks. The residues from the filter were transferred into a beaker (2 l) by leaching with 120 ml of 0.02 M nitric acid and 80 ml of water.

Stage 4 (SIV): 100 ml of 30 % hydrogen peroxide acetified with nitric acid up to pH 2 was added to the beaker which contained the suspension from the SIII. The control testing solution comprised acidic solution of hydrogen peroxide. The beaker was covered with a watch glass and treated for 120 min in a heated bath at 85 °C, with periodical mixing. Then, additional 60 ml of the acidic hydrogen peroxide solution was added and the suspension was heated for another 3 hours with occasional stirring. Upon cooling, in order to conduct desorption, 100 ml of 3.2 M ammonium acetate was added to the solution. Required concentration (1 M) was obtained by adding water up to 500 ml. The suspensions were mixed on a rotary mixer for 30 min, after which they were rested for a minimum of 12 hours. Filtration and leaching were conducted using the same principle from the previous phases (i.e., negative reaction on ammonium ions). The obtained solutions were concentrated up to 400 ml, diluted to 500 ml and poured into hermetically sealed plastic flasks.

Stage 5 (SV): 5 g of dried residue from the SIV was mixed with 20 ml of concentrated nitric acid, 10 ml of concentrated hydrochloric acid and 20 ml of concentrated hydrofluoric acid. Precipitation was carried out for 120 minutes at 140 °C. Upon cooling, the suspension was heated up to 210 °C, and then re-suspended in 50 ml of 0.5 M chloric acid. The solutions were filtrated and poured into volumetric flasks, diluted up to 100 ml and transferred into hermetically sealed plastic flasks.

2.2 Instrumental methods

Four analytical techniques were employed: X-ray fluorescence (XRF), inductively coupled plasma optical emission spectrometry (ICP-OES), inductively coupled plasma mass spectrometry (ICP-MS), and atomic absorption spectroscopy (AAS). The XRF technique was used on the solid samples, i.e. the initial powdery ash. AAS and ICP techniques used the diluted ash samples. The following targeted trace elements were investigated: As, Ga, Ce, Be, Ge, Nd, Cr, Zr, Eu, Cu, Nb, Gd, Co, Mo, Dy, Li, Ag, W, Mn, Cd, Au, Ni, In, Hg, Pb, Sn, Tl, V, Sb, Th, Zn, and La.

X-ray fluorescence analysis was conducted on an XRF spectrometer (ED 2000, Oxford). The initial ash powdery samples were pressed into solid pellets with 2.5 cm diameter. A reference material SRM 1633b NIST was used for the calibration. Atomic absorption spectroscopy of the diluted samples was performed via AAS spectrometer (3100, Perkin Elmer). Inductively coupled plasma optical emission spectrometry was performed on an ICP-OES spectrometer (SPECTRO BLUE TI - SPECTRO Analytical Instruments GmbH). Inductively coupled plasma mass spectrometry measurements were conducted on an ICP-MS apparatus (iCAP Q, Thermo Scientific X series 2). For the calibration, a multi-element ICP standard (Roth Carl) and periodic table mix 1 ICP were used. The metal elements were detected using standard reference materials: SRM 1633b NIST, SRM 2689 NIST, 2690 NIST,

2691 NIST, and CRM012 - Sigma-Aldrich. RTC standard reference material 1633c (NIST) were digested in triplicate and analyzed to acquire the quality assurance. All measurements (obtained in triplicate) were expressed as a mean value with standard deviation.

2.3 Statistical analyses

Principal component analysis (PCA) was used to discover the possible correlations among the measured parameters. PCA is a central tool in exploratory data analysis. It is a multivariate technique where data are transformed into orthogonal components that are linear combinations of the original variables. PCA is done by Eigenvalue decomposition of a data correlation matrix. The first component has the largest possible variance in this transformation. The analysis is used to achieve maximum separation between parameter clusters [44]. This approach, evidencing spatial relationship between processing parameters, enabled a differentiation between different samples. Cluster analysis (CA) is used to classify objects into groups. The cluster analysis of the samples is illustrated as dendrograms. All determinations were made in triplicate. The data were processed statistically using the software package STATISTICA 10.0 (StatSoft Inc., Tulsa, OK, USA).

3. Results and Discussion

Upon sampling of the coal ash from the boreholes B4, B7, B12, B15, B19, and B22, untreated powders were submitted to the X-ray fluorescence analysis. The obtained results are presented in the Table I (main elements) and Table II (traces elements).

Tab. I The main elements comprised in coal ash samples from the TENT-A landfill.

Oxide, %	B4				B7				B12			
	5m	10 m	15 m	19 m	5m	10 m	15 m	19 m	5m	10 m	15 m	19 m
Al ₂ O ₃	22.69	19.01	20.37	21.18	20.13	19.92	20.56	21.22	18.98	20.57	24.07	21.64
SiO ₂	48.45	52.53	52.17	50.59	50.52	51.55	50.22	49.75	54.49	52.53	48.28	49.83
CaO	5.95	6.68	6.08	7.61	6.14	7.21	7.35	7.18	6.34	6.37	7.12	7.15
Fe ₂ O ₃	7.79	5.71	5.62	6.20	7.80	6.29	6.55	6.61	7.67	5.70	5.22	6.26
Na ₂ O	0.19	0.73	0.38	0.44	0.29	0.47	0.36	0.39	0.22	0.49	0.36	0.89
MgO	1.71	1.57	1.60	2.14	1.46	2.12	1.74	1.65	1.44	1.62	1.39	1.54
P ₂ O ₅	0.07	0.07	0.06	0.03	0.06	0.07	0.03	0.05	0.07	0.06	0.08	0.07
MnO	0.05	0.05	0.05	0.03	0.05	0.04	0.04	0.05	0.04	0.05	0.07	0.05
K ₂ O	0.98	0.96	1.29	1.22	1.72	1.21	1.34	1.56	1.52	0.98	0.95	1.67
TiO ₂	0.60	0.54	0.59	0.52	0.56	0.46	0.53	0.57	0.58	0.59	0.47	0.63
Oxide, %	B15				B19				B22			
	5m	10 m	15 m	19 m	5m	10 m	15 m	19 m	5m	10 m	15 m	19 m
Al ₂ O ₃	20.39	19.74	19.82	20.90	21.02	20.68	20.35	20.64	21.18	21.38	20.92	20.94
SiO ₂	50.64	53.53	52.59	49.69	50.59	50.95	52.51	50.89	50.32	49.62	51.21	50.94
CaO	6.85	5.42	5.98	6.48	7.10	6.81	6.59	6.38	7.11	7.23	6.92	6.81
Fe ₂ O ₃	7.21	5.66	6.29	7.81	6.37	7.22	6.95	6.52	6.87	7.12	6.68	6.90
Na ₂ O	0.39	0.52	0.36	0.47	0.48	0.36	0.38	0.41	0.49	0.55	0.36	0.38
MgO	1.53	1.37	1.29	1.43	1.74	1.48	1.35	1.88	1.65	1.92	1.49	1.67
P ₂ O ₅	0.06	0.07	0.07	0.06	0.03	0.04	0.04	0.06	0.04	0.04	0.05	0.07
MnO	0.05	0.07	0.06	0.06	0.04	0.05	0.06	0.05	0.05	0.05	0.04	0.04
K ₂ O	1.71	1.54	1.60	1.64	1.32	1.45	1.29	1.55	1.18	0.99	1.29	1.38
TiO ₂	0.55	0.57	0.52	0.58	0.56	0.59	0.46	0.51	0.55	0.59	0.63	0.58

Tab. II The trace elements comprised in coal ash samples from the TENT-A landfill.

Element mg/kg	B4				B7				B12			
	5m	10 m	15 m	19 m	5m	10 m	15 m	19 m	5m	10 m	15 m	19 m
V	130.3	111.0	136.4	144.2	121.8	118.9	139.5	141.1	137.9	113.7	110.6	125.0
Cr	146.9	129.8	133.6	148.1	125.0	132.1	144.3	129.5	139.5	135.6	120.9	136.9
Co	13.7	18.4	15.2	16.2	13.2	19.1	18.5	14.3	15.0	15.4	14.0	11.3
Ni	64.0	50.2	58.3	41.3	52.4	64.3	54.8	71.9	71.6	61.3	54.7	69.1
Cu	41.0	37.2	44.1	26.0	31.2	36.3	42.8	59.5	41.6	46.4	71.2	52.3
Zn	60.8	40.8	47.0	36.1	42.3	74.1	58.8	49.2	56.5	44.2	74.0	55.3
Ga	14.3	11.4	14.3	16.3	11.9	18.1	14.2	18.6	19.5	14.0	29.1	17.0
As	25.4	19.9	22.2	22.4	12.1	19.5	34.6	26.3	20.4	24.0	22.9	41.0
W	16.8	89.6	23.8	24.5	38.4	21.8	26.9	18.2	23.0	10.0	14.7	21.2
Zr	33.6	40.8	41.3	40.9	41.1	31.8	45.1	36.2	47.0	38.2	36.3	55.0
Pb	24.7	19.9	23.5	19.1	19.4	20.4	21.6	19.7	21.5	19.5	22.7	31.3
Th	9.0	7.7	9.1	10.2	9.8	8.5	8.9	10.1	10.7	7.7	7.1	13.3
Nb	5.0	4.5	5.7	5.9	5.1	6.4	7.1	7.2	6.8	4.8	4.5	7.9
Mo	0.2	0.3	0.6	0.7	ND	0.1	0.4	ND	0.2	0.3	0.4	ND
Ag	0.5	0.8	0.4	0.2	ND	0.1	ND	0.1	0.3	0.1	0.3	0.1
Cd	0.4	ND	ND	ND	0.2	ND	ND	ND	ND	0.012	0.4	ND
In	0.1	0.3	0.2	0.2	ND	ND	0.1	0.1	0.3	0.1	ND	0.1
Sn	1.5	0.9	0.9	1.8	1.1	1.9	1.5	1.1	1.8	1.2	1.6	1.6
Sb	1.0	1.2	0.4	0.6	0.5	0.8	1.1	0.6	0.9	1.0	0.4	1.0
La	0.5	4.9	ND	8.2	3.4	5.9	2.8	6.3	8.3	8.1	5.6	ND
Ce	15.0	28.6	32.6	19.6	28.9	21.9	30.2	19.4	20.8	21.4	18.3	16.7
Nd	17.8	11.5	18.5	10.6	4.6	14.2	19.1	18.2	12.4	6.8	10.4	22.3
Tl	0.8	0.5	0.7	0.9	0.6	0.8	0.3	0.6	0.6	0.6	0.5	0.5
Element mg/kg	B15				B19				B22			
	5m	10 m	15 m	19 m	5m	10 m	15 m	19 m	5m	10 m	15 m	19 m
V	120.7	84.9	96.2	123.6	111.6	125.3	96.8	102.6	119.3	108.8	93.8	115.5
Cr	129.6	219.9	132.2	136.5	148.1	184.2	165.1	138.6	149.2	118.8	154.9	129.7
Co	12.9	18.3	15.6	12.3	18.6	20.1	13.2	18.3	11.9	19.5	21.2	18.4
Ni	61.5	47.7	48.6	58.5	41.3	49.6	58.1	62.6	55.9	48.2	71.6	64.9
Cu	46.4	29.9	37.1	46.9	26.8	41.6	40.8	35.7	33.3	39.8	54.2	48.1
Zn	46.3	36.6	34.2	47.7	36.6	44.6	50.1	58.4	32.5	40.6	38.4	46.2
Ga	16.5	10.2	13.8	15.1	19.1	18.3	22.6	18.8	15.9	18.5	21.3	18.3
As	24.2	5.4	8.8	21.9	13.8	19.1	25.9	30.7	18.1	20.6	16.8	29.7
W	28.5	67.0	62.3	31.9	38.9	44.1	26.9	60.8	61.2	48.7	39.8	45.6
Zr	36.4	48.4	35.9	44.6	55.4	38.6	31.9	48.7	60.2	54.7	61.5	39.7
Pb	20.8	17.8	15.4	18.5	15.1	18.7	16.4	14.3	17.8	18.5	19.6	20.2
Th	7.7	6.5	5.3	8.6	9.2	10.1	8.6	7.8	8.5	10.4	9.3	9.7
Nb	4.9	4.8	4.2	5.2	7.4	8.1	6.3	5.2	4.9	8.3	8.7	7.3
Mo	0.1	ND	0.3	0.3	0.2	0.5	0.1	0.1	0.2	0.4	0.1	0.2
Ag	0.03	0.5	0.4	0.3	ND	0.1	0.2	0.1	0.1	ND	0.1	0.1
Cd	0.3	ND	ND	ND	ND	ND	0.2	ND	0.1	ND	ND	ND
In	0.2	0.2	0.3	0.2	0.3	0.2	0.1	0.2	0.3	0.3	0.3	0.2
Sn	1.6	1.0	1.1	1.3	1.8	1.4	1.9	2.2	1.5	1.8	1.1	1.7
Sb	0.7	0.6	0.7	0.4	0.1	0.5	0.4	0.7	0.8	0.1	0.4	0.3
La	6.6	5.6	4.3	4.0	5.7	6.2	7.1	5.6	5.9	6.2	6.6	7.3
Ce	23.5	14.3	14.4	21.9	20.5	18.3	17.9	22.4	25.6	19.7	17.9	20.1
Nd	19.3	8.9	18.2	10.9	14.7	20.1	18.1	17.0	15.9	18.2	19.9	17.5
Tl	0.6	0.6	0.7	0.8	0.9	0.8	0.9	0.7	0.6	0.8	0.8	0.7

*ND – not detected

Even though the XRF analysis of the main oxides did not show major differences between the samples originating from different sampling positions, there were notable variations in the concentrations of the trace elements detected in the samples from different boreholes and different sampling depths. The elements Hg, Ge, Gd, Eu, Dy, and Au could not be detected on the starting coal ash sample by XRF method. The following thirty two elements - As, Ga, Ce, Be, Ge, Nd, Cr, Zr, Eu, Cu, Nb, Gd, Co, Mo, Dy, Li, Ag, W, Mn, Cd, Au, Ni, In, Hg, Pb, Sn, Tl, V, Sb, Th, Zn, and La, were selected as elements of interest and therefore they were further analyzed. Namely, the variations in concentrations of the mentioned elements were monitored after each of five stages of the extraction. The diluted samples were analyzed via AAS and ICP. The summarized results are illustrated in Fig. 2.

The total sum of arsenic obtained upon all five stages of the extraction varied between 16.35 mg/kg and 85.30 mg/kg depending on the position and depth of the sampling site. The

samples acquired from the deepest points of the boreholes (i.e. 19 m) had the highest concentrations of arsenic. Stage three (SIII) of the extraction produced the highest concentrations of As in all samples. The highest amount of As upon singular extraction was 55.91 mg/kg and it was obtained from the sample B22-19 during the SIII phase.

The stages I and II of beryllium extraction produced extremely small quantities of this element. The stage II proved to be somewhat more efficient, i.e. the abundance of Be extracted from the ash sample in SII was at least 20 times higher than that of SI phase. However, the highest concentrations of Be were obtained during the stage SIV (mean value = 77.7 mg/kg). The highest Be content was acquired at the B22-19 site during SIV stage (130.9 mg/kg). The total sum of Be concentrations was in the range from 2.4 mg/kg to 5.2 mg/kg. The concentrations were not significantly varying with regard to the borehole position or depth. At least 60-80 % of total Be concentration originated from the coal ash amorphous phase.

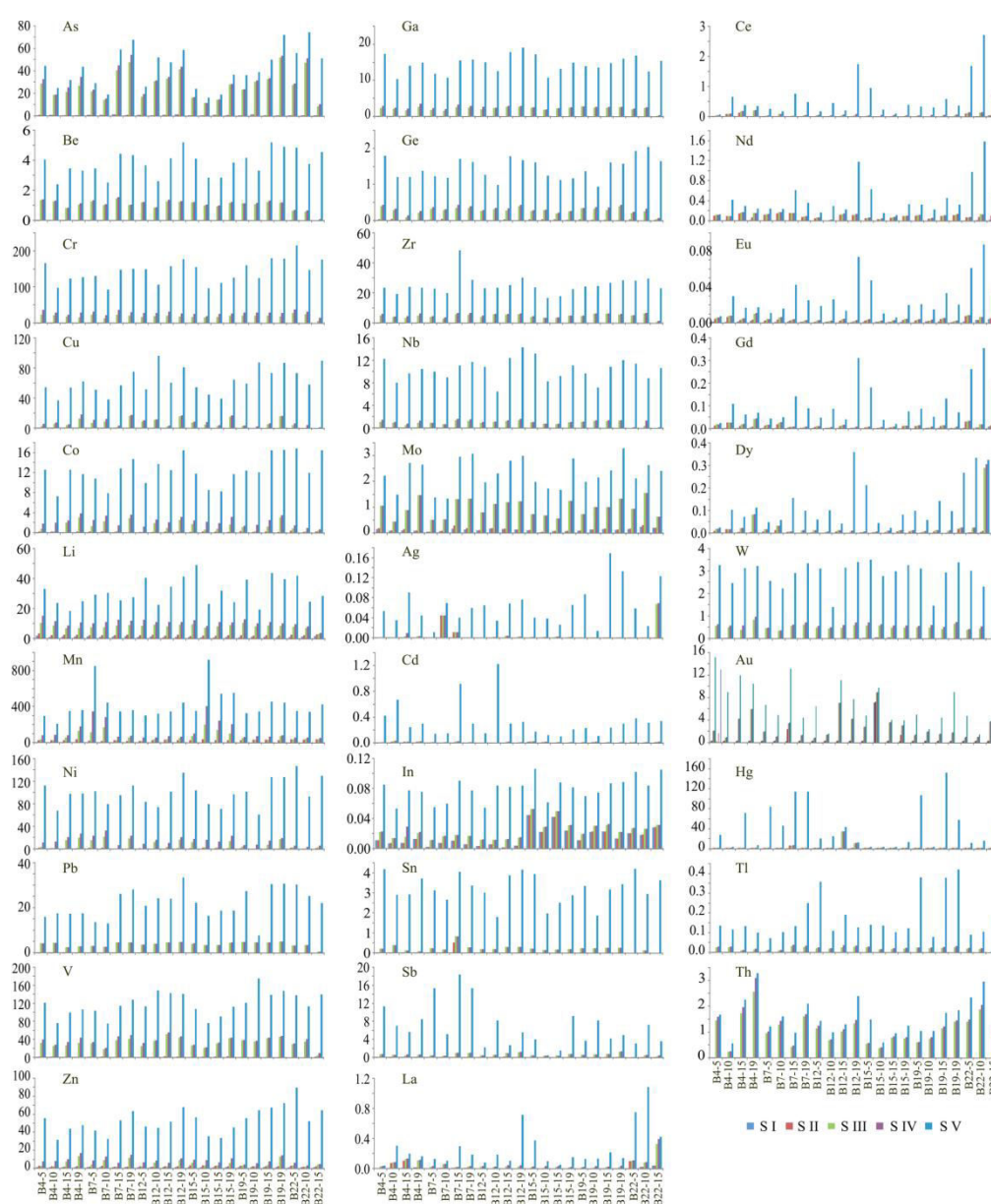


Fig. 2. Concentrations of the elements obtained upon each extraction stage.

Chromium concentrations obtained during SI and SII were extremely variable: from hardly detectable concentrations ($< 0.1 \mu\text{g/kg}$) to higher values, e.g. $208.5 \mu\text{g/kg}$ (B7-10, SII). Stages III and IV were more uniform with mean values of about 20 mg/kg and 10 mg/kg , respectively. The stage V produced the highest concentrations of Cr (predominantly above 80 mg/kg). The highest concentration of Cr was extracted from the B19-19 sample during SV (179.99 mg/kg). The total sum of the Cr concentrations (all five stages) varied between a minimum of 52.34 mg/kg to maximum of 415.53 mg/kg , mean value being 147.31 mg/kg .

Copper had an unsteady stage I extraction with extremely variable and/or hardly detectable results. The stage SII was more stable, namely the detected concentrations varied from $41.6 \mu\text{g/kg}$ (B12-10) to $159.7 \mu\text{g/kg}$ (B19-5). SIII and SIV produced relatively low Cu concentrations ($< 10 \text{ mg/kg}$), while SV was highly satisfactory with the mean concentration being approximately 60 mg/kg . The total sum of the Cu concentrations (all five stages) extended from 37.33 mg/kg to 96.23 mg/kg . The concentration mean value was 59.98 mg/kg . At least 70-90 % of Cu was found in the ash amorphous phase.

Cobalt exhibited a very low abundance in the samples upon I – IV extraction stages. The acquired Co concentrations were below 10 mg/kg . The concentrations reached after the stage V were predominantly higher than 10 mg/kg . The SV phase gave the highest concentrations which ranged from 4.53 mg/kg (B7-10 sample) to 15.79 mg/kg (B22-15 sample). The total sum of the Co concentrations (all five stages) varied between 7.35 mg/kg and 16.82 mg/kg , while the obtained mean value was 12.48 mg/kg . Easily mobile Co concentrations ($1\text{-}300 \mu\text{g/kg}$) were present only in the stages I and II, while 50-90 % of total Co quantity were within the ash amorphous phase.

SI to SIV stages produced very low lithium concentrations. The fifth extraction stage resulted with more acknowledgeable concentrations, i.e. from 9.27 mg/kg (B19-9) to 36.74 mg/kg (B15-5). The total sum of the Li concentrations during all five stages varied from 18.58 mg/kg and 49.08 mg/kg . Mean value was 28.88 mg/kg . At least of 50 % of total Li quantity was within the ash amorphous phase.

The quantity of manganese obtained in the stage was lower than 2 mg/kg . The concentrations progressively increased during stages II, III and IV, and reached the highest values in the stage V (from 124.51 mg/kg (B4-10) to 514.08 mg/kg (B15-10)). The total sum of the manganese concentrations upon all five stages varied from 212.45 mg/kg to 922.24 mg/kg . Mean value was 356.91 mg/kg . At least of 30 – 80 % of total Mn quantity was in ash amorphous phase.

The obtained concentrations of nickel followed the same pattern of the manganese extraction. Namely, Ni concentrations obtained during the stages SI-IV hardly surpassed 10 mg/kg . Concentrations acquired during SV were between 53.43 mg/kg (B19-19) and 140.90 mg/kg (B22-5). Total sum of the Ni concentrations upon all five stages was between 61.39 mg/kg and 147.11 mg/kg , with mean value of 100.44 mg/kg . At least of 75-80 % of total Ni was found in amorphous phase of the coal ash. Pb, V, Zn and Ga exhibited the same behavior as Mn and Ni by showing the highest concentrations during the last stage of the extraction (SV). The sums of the Pb concentrations varied between 7.90 mg/kg and 33.44 mg/kg , with mean value of 22.21 mg/kg (40-80 % of total Pb originated from the ash amorphous phase). The sums of the V, Zn and Ga concentrations ranged from 75.77 mg/kg to 175.27 mg/kg , 30.24 mg/kg to 369.36 mg/kg , and 10.46 mg/kg to 19.15 mg/kg , respectively. At least 70 % of these elements originated from the ash amorphous phase.

Germanium, zirconium, niobium, mercury and antimony were extracted in moderately significant amounts only during the SV. All phases conducted prior to the fifth stage resulted with concentrations of these elements lower than 1 mg/kg . The total sums of the Ge, Zr, Nb, Hg and Sb concentrations varied between 0.94 mg/kg and 2.05 mg/kg , 16.62 mg/kg and 47.51 mg/kg , 6.51 mg/kg and 14.34 mg/kg , 4.6 mg/kg and $149.5 \mu\text{g/kg}$, and 0.5 mg/kg and 18.44 mg/kg , respectively. 70-90 % of these elements, i.e. Ge, Zr and Nb, originated from the ash amorphous phase. Mercury was extremely irregularly associated with

the ash. The association with the glassy phase was in a very narrow diapason from 90 % to 100 %. 60-90 % of Sb was associated with amorphous phase.

Identified concentrations of Mo, Ag, Cd, In, Sn, La, Ce, Nd, Eu, Gd, Dy, W, Au, Tl, and Th were very low during all five stages of the extraction. The obtained quantities of these elements were especially low during the initial extraction stage. There were smaller alternations in their behavior, like in the case of Sn, La, or Ce which all exhibited an increase in their concentrations after the SIII. Or in the case of Nd and Gd, the stage II produced higher concentrations. However, the trend of productivity during individual stages implies that for all of the mentioned elements full five stage extractions are obligatory. The total sums of the Mo, Ag, Cd, In, and Sn concentrations varied between 1.53-3.52 mg/kg, 0.01 - 0.17 mg/kg, 0.10 - 1.23 mg/kg, 0.05 - 0.11 mg/kg, and 1.81 - 4.21 mg/kg, respectively. 40 - 60 % of Mo was associated with the amorphous phase in the coal ash. 100 % of silver was in the glassy phase. The majority of Cd and Sn (90 %) were also associated with the amorphous phase, while this percentage for In varied between 45 - 80 %. The summed quantities of La, Ce, Nd, Eu, Gd, Dy, W, Au, Tl, and Th after all five extraction stages were as follows: 0.04 - 1.09 mg/kg, 0.07 - 2.73 mg/kg, 0.11 - 1.53 mg/kg, 0.01 - 0.09 mg/kg, 0.02 - 0.35 mg/kg, 0.02 - 0.36 mg/kg, 1.42 - 3.52 mg/kg, 0.5 - 14.7 μ g/kg, 0.07 - 0.42 mg/kg, and 0.57 -3.29 mg/kg. 90 % of La was associated with amorphous phase in the ash. Wolfram was 55 – 90 % associated with ash glassy phase, while this percentage for thallium was even higher, i.e. 70 –90 %. Ce, Nd, Eu, Gd and Dy were highly irregularly associated with the ash compounds, but their associations were predominantly related to the coal ash amorphous phase.

The mean values of the concentrations of all 32 investigated elements obtained from the TENT-A landfill coal ash are summarized in Table III. The presented concentrations are mean values acquired after all 5 stages of extraction.

Tab. III Obtained mean values (MV) of concentration of 32 elements upon five stage extraction.

Element	As	Be	Cr	Cu	Co	Li	Mn	Ni
MV, mg/kg	44.34	3.97	147.31	59.98	12.48	28.88	356.91	100.44
Element	Pb	V	Zn	Ga	Ge	Zr	Nb	Mo
MV, mg/kg	22.21	117.85	52.84	14.90	1.44	23.98	10.38	2.61
Element	Ag	Cd	In	Sn	Sb	La	Ce	Nd
MV, mg/kg	0.06	0.30	0.08	3.15	5.60	0.18	0.39	0.33
Element	Eu	Gd	Dy	W	Au	Hg	Tl	Th
MV, mg/kg	0.02	0.08	0.10	3.01	$4.5 \cdot 10^{-3}$	$41.9 \cdot 10^{-3}$	0.13	1.47

Since only arsenic and beryllium showed the maximal concentrations during earlier stages of the extraction (SIII for As and SIV for Be), it can be adopted that all elements have to go through all five stages of the planned procedure. The obtained data of the chemical analyses upon the fifth stage of extraction are further correlated with the characteristics of the TENT-A landfill. Namely, the spatial and depth dispositions of the concentrations of investigated elements (As, Ga, Ce, Be, Ge, Nd, Cr, Zr, Eu, Cu, Nb, Gd, Co, Mo, Dy, Li, Ag, W, Mn, Cd, Au, Ni, In, Hg, Pb, Sn, Tl, V, Sb, Th, Zn, and La) on the coal combustion ash landfill were assessed and interrelated.

In order to express the concentration profile within the print shop, the general convection–diffusion equation can be written. It is a combination of the diffusion and convection equations, and it describes concentration space distribution inside a physical system due to two processes: diffusion and convection. During this investigation, an assumption was made, and diffusion coefficient is considered constant, with no sources or sinks, and with velocity field for an incompressible fluid. The equation was written in the following form:

$$\frac{\partial c}{\partial t} = D\nabla^2 c - \vec{v} \cdot \nabla c \quad (1)$$

Another assumption can be made, for the stationary behavior of a convective-diffusive system, where steady state of system is involved. In the steady state, $\partial c / \partial t = 0$, with no velocity field, $\vec{v} = 0$, the above formula is derived to:

$$-D\nabla^2 c = 0 \quad (2)$$

The two-dimensional concentration field is discretized in Cartesian coordinates. Numerical grids are made from 19,540 control volumes. Optimization of the numerical grid was performed, and grid refinement test showed that there is no significant change in the results of the simulation for larger number of cells in control volume. Elements used in numerical mesh are triangular and size of an element is less than 10^{-8} m^3 .

The distribution patterns of the contents of each analyzed element from the TENT-A landfill are shown in Fig. 3.

From the Fig. 3, it can be seen that the content of As showed a generally increasing trend. The As concentrations at the lowest drilling points (19 m) on the landfill were higher than its concentrations at the initial positions (5 m). For example, the As concentration at the borehole B12 measured at 5 m depth was 26.34 mg/kg, while the concentration at 19 m depth reached 58.80 mg/kg. A similar trend was observed for all other sampling positions, which means that As has a highly pronounced migration ability as it is easily leached by atmospheric water. Thereby, the highest percentage of arsenic was accumulated at the bottom of the landfill. Copper exhibited highly similar behavior as arsenic, having the highest concentrations registered at the lowest sampling points. The other elements that followed this pattern of behavior were: lead, vanadium, zinc, molybdenum, lanthanum, cesium, europium, dysprosium, and thorium. The borehole B22 was characterized by the highest contents of As, Cu, Ce, Eu, Zn, Dy, and Th. The samples with the highest La content were extracted from the borehole B15. The most abundant elements on the B12, B19 and B4 positions were Pb, V, and Mo, respectively. Lithium showed the opposite pattern of behavior than the previously described elements. Namely, Li exhibited a predominantly decreasing trend regarding concentrations with respect to the depth of the boreholes. The highest decrease (50 %) of the Li concentration was observed at B12 and B22.

The other group of elements showed small and irregular variations in their concentrations regarding the depth of a borehole. Namely, a clearly either increasing or decreasing trend could not be identified. The concentrations of beryllium insignificantly varied between 3.5 mg/kg and 4.5 mg/kg (i.e., the mean value was 3.97 mg/kg) for all the sampling positions as well all of the sampling depths. Chromium displayed approximate concentration of 140 mg/kg for all sampling dispositions. The only 'anomaly' in its behavior was displayed at B22 where the initial concentration of 215.5 mg/kg decreased four times in regard to the depth of the sampling borehole, only to reach the final concentration of 52.33 mg/kg. Cobalt showed a steady trend of either small increase or decrease with the depth of a borehole thereby maintaining the mean value of 12.48 mg/kg. The highest concentrations of Co were observed at B19 and B22 dispositions. Manganese exhibited extremely huge gap between the initial and the final values of concentration at B7 (845.5 – 365.2 mg/kg) and B15 (353.05 - 552.1 mg/kg). Ni had mean value which oscillated around 100 mg/kg. The highest nickel concentrations were measured at positions B12-19 and B 22-5. Similar to cobalt, Ga, Ge, Zr, Nb, and Ag showed very small oscillations among the concentrations measured at different depths and different locations. The mean values for gallium, germanium, zirconium, niobium, and silver were: 14.90, 1.44, 23.98, 10.38, and 0.06 mg/kg. Ga was most abundant at B12 and B15 dispositions, Zr and Ge at B22, and Nb at B15. The concentrations of Cd, In, Sn, Sb, Nd,

Gd, W, Au, and Tl did not significantly vary with respect to the depth and/or disposition of a sampling point. The highest cadmium concentration was observed at B4-10 (0.67 mg/kg), while the mean value was 0.30 mg/kg. Indium was the most abundant at the B22 disposition (0.102-0.089 mg/kg). Tin (Sn) maintained its mean value 3.15 mg/kg for all borehole dispositions. Antimony showed the highest concentrations at B7 and the lowest at B12 borehole. Its mean value was 5.60 mg/kg. Neodymium had maximal concentration at B22-10 disposition (1.52 mg/kg), while its mean value was 0.33 mg/kg. The concentrations of Gd were very low at all dispositions (mean value = 0.08 mg/kg), save for the B22 sampling point: 0.2-0.35 mg/kg. Wolfram and thallium showed small variations between their sampling points. Mean values of concentration for W and Tl were 3.01 mg/kg and 0.13 mg/kg, respectively. Au was especially high at B4 (14.7-9.98 $\mu\text{g/kg}$), although its mean concentration was 4.50 $\mu\text{g/kg}$.

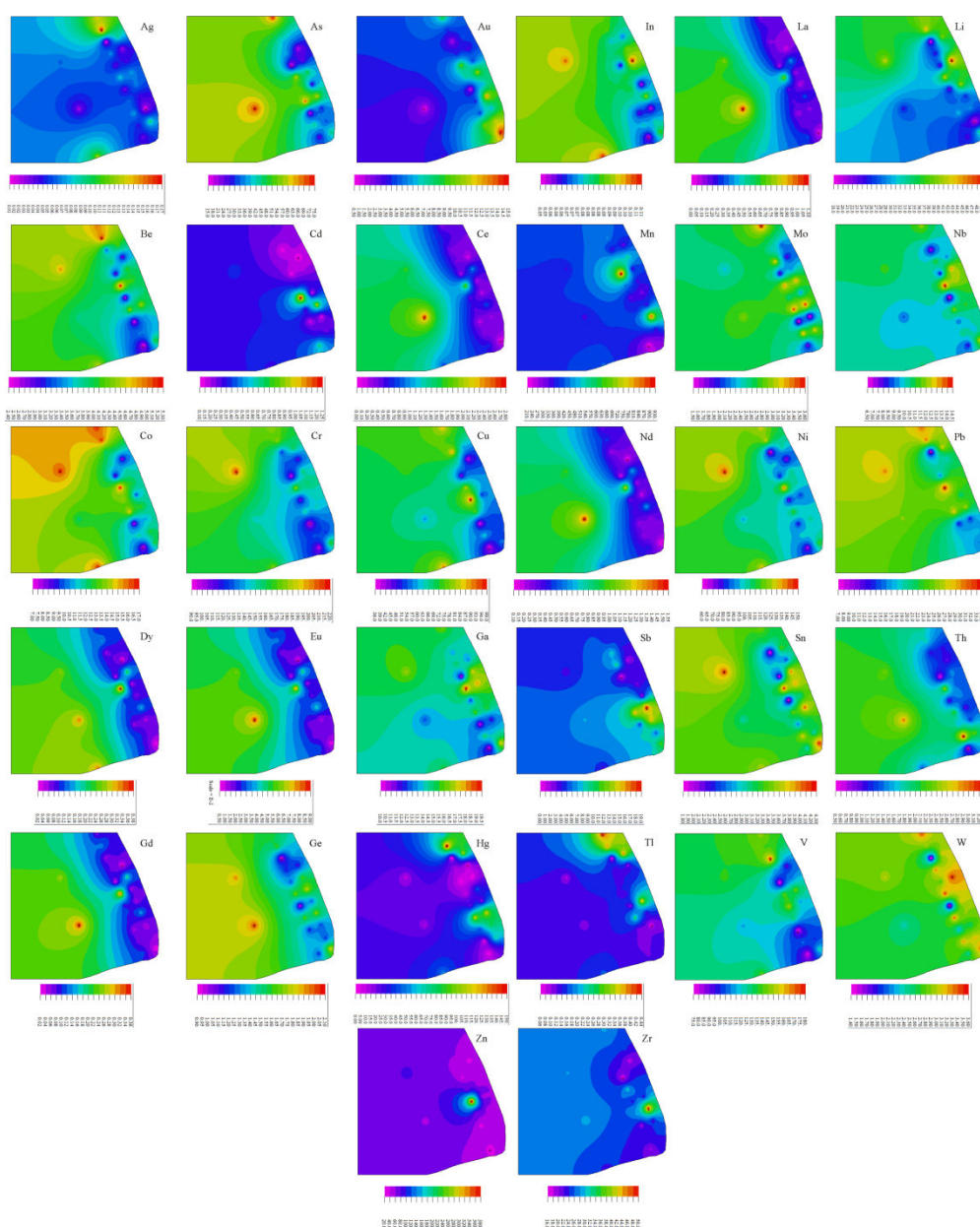


Fig. 3. Distribution patterns of analyzed elements identified on the TENT-A landfill.

Mercury, which was not detected via XRF analysis in the initial ash sample (Table III), was identified upon conducted extraction, but the concentrations were infinitesimal. The registered concentrations of Hg on the landfill showed certain variations. The concentration of mercury sampled on the B4 site decreased from 25.08 $\mu\text{g}/\text{kg}$ to 4.46 $\mu\text{g}/\text{kg}$. Contrarily, on the B7 disposition the concentration increased with increasing borehole depth from 81.7 $\mu\text{g}/\text{kg}$ to 111.69 $\mu\text{g}/\text{kg}$. At B15 disposition the registered concentration of Hg was only 0.3 $\mu\text{g}/\text{kg}$. The mean value of Hg concentration for entire landfill was 41.90 $\mu\text{g}/\text{kg}$.

3.1 Mathematical analysis of correlations established between identified trace elements upon five stage extraction

The concentration data set of chemical compounds obtained during five stages of extraction from the coal ash samples was further submitted to the mathematical analysis via STATISTICA 10.0 software package. Thirty two elements have been analyzed. The data were mathematically analyzed and evaluated by in order to determine the average concentrations of elements and to perceive their variability.

The Table IV presents significant correlations between 32 investigated trace elements. All given correlation are statistically significant at $p < 0.01$ level. Arsenic is correlated with sixteen elements: Be, Cr, Cu, Co, Ni, Pb, V, Zn, Ge, Zr, Mo, Ce, Nd, Eu, Gd, and Dy. Correlation coefficients are ranging from 0.530 to 0.775. This means that As is likely to be found accompanied by the mentioned elements in the coal ash. The highest obtained correlation coefficients are 0.775 for cobalt and 0.759 for molybdenum, which means that arsenic is strongly connected with these two elements. Arsenic has a strong correlation with five REE: Ce, Nd, Eu, Gd, and Dy. Beryllium is associated with Cr, Co, Li, Ni, Pb, V, Zn, Ga, Ge, Zr, Nb, Mo, In, Sn, and W. Correlation coefficients are ranging from 0.559 to 0.925. Be exhibits the strongest correlation with chromium. However its correlations with REE are not statistically significant. Chromium is correlated with Co, Li, Ni, Pb, V, Zn, Ga, Ge, Nb, In, Sn, and Dy. The correlation coefficients are varying from the lowest value obtained for Dy (0.539) to the highest value exhibited for Zn (0.901). Dy is the only REE significantly correlated to Cr. Copper is correlated with Co (0.822), V (0.894) and Zn (0.700). It shows no significant correlations with REE. Cobalt is associated with the following elements: Ni, Pb, V, Zn, Ga, Ge, Mo, In, and Dy. The registered significant correlation coefficients are ranging from 0.537 to 0.889. Dy is the only REE correlated with cobalt. Lithium is correlated with Ni, Pb, Ga, Nb, Sn, and W with coefficient oscillating in the very narrow interval: 0.534-0.669. Nickel is related to: Pb, Zn, Ga, Ge, Nb, In, Sn, Dy, and W. The correlation coefficient established with Dy is 0.560. Pb is correlated with Zn, Ga, Ge, Nb, and four REE (Nd, Eu, Gd, and Dy). The correlation coefficients with REE are in the 0.541 - 0.580 interval. Vanadium is associated with Zn and Ga. Zinc is correlated with Ga, Ge, In, and Dy as the only REE in this group (correlation coefficient 0.523). Ga is not associated with REE by statistically significant correlations, but it is correlated with Ge, Nb, Mo, In, Sn, and W. The correlation with Nb is especially strong (0.862). Germanium is strongly correlated with five REE: La (0.622), Nd (0.651), Eu (0.634), Gd (0.639), and Dy (0.604).

The rest of significant correlations Ge established with Nb, In, and Sn. Zr is correlated only with Mo and Sb, Nb with Sn, and Sn with W. Indium is associated with Dy as REE with correlation coefficient 0.549. Lanthanum is strongly correlated with the rest of REE: Ce (0.994), Nd (0.983), Eu (0.966), Gd (0.968) and Dy (0.897). Correlations of Ce with Nd, Eu, Gd and Dy are 0.990, 0.972, 0.965 and 0.880, respectively. A REE neodymium is correlated with Eu (0.985), Gd (0.979) and Dy (0.905). Europium has high correlation coefficients in association with Gd (0.990) and Dy (0.935). Finally, Gd is correlated to Dy with coefficient as high as 0.968. Mercury is only correlated with thallium (0.536).

From the correlations presented in Table IV, it can be seen that investigated REE (La, Ce, Nd, Eu, Gd, Dy, and Nd) are strongly connected, showing correlation coefficients higher than 0.880. These interrelations were anticipated. However, the elements found in the coal combustion ash, such as As, Pb, and Ge, have relatively strong correlations with a number of REs: Nd, Eu, Gd, Dy, and also La in case of Ge, as well as Ce in case of As. Neodymium was especially strongly correlated with other REE. Dysprosium showed the most abundant correlations, since it was associated both with REE and the number of trace elements (As, Cr, Co, Ni, Pb, Zn, Ge, and In).

Tab. IV Correlation coefficients between trace elements content in the coal ash samples.

	Be	Cr	Cu	Co	Li	Ni	Pb	V	Zn	Ga	Ge	Zr	Nb	Mo	In	Sn	Sb	La	Ce	Nd	Eu	Gd	Dy	W	Tl
As	0.645	0.610	0.673	0.775		0.563	0.670	0.638	0.680		0.648	0.659		0.759					0.546	0.571	0.555	0.547	0.530		
Be		0.925		0.856	0.606	0.881	0.746	0.575	0.844	0.791	0.703	0.564	0.767	0.588	0.587	0.709									0.559
Cr				0.830	0.668	0.884	0.700	0.598	0.901	0.779	0.750		0.691		0.615	0.740								0.539	
Cu				0.822				0.894	0.700																
Co						0.834	0.710	0.769	0.889	0.676	0.537			0.625	0.660										0.556
Li						0.576	0.569			0.565		0.669			0.561										0.534
Ni							0.697		0.783	0.690	0.709	0.743		0.565	0.752										0.560
Pb									0.617	0.549	0.622	0.532							0.541	0.580	0.571	0.559			0.576
V									0.758	0.566															
Zn										0.686	0.587				0.625										0.532
Ga											0.591		0.862	0.629	0.635	0.770									0.626
Ge													0.639		0.542	0.773		0.622		0.651	0.634	0.639	0.604		
Zr														0.627			0.562								
Nb																	0.862								
In																									0.549
Sn																									0.710
La																			0.994	0.983	0.966	0.968	0.897		
Ce																				0.990	0.972	0.965	0.880		
Nd																					0.985	0.979	0.905		
Eu																						0.990	0.935		
Gd																							0.968		
Hg																									0.536

A dendrogram of trace elements content, including REE, identified in the ash samples upon the fifth stage of extraction, using complete linkage as an amalgamation rule and the City Block (Manhattan) distance as a measure of the proximity between samples is shown in Fig. 4. The dendrogram based on ICP data showed a proper distinction between samples. The type of sample influenced the position of this sample in factor space. As shown in Fig. 4, there is similarity in samples grouped in various clusters.

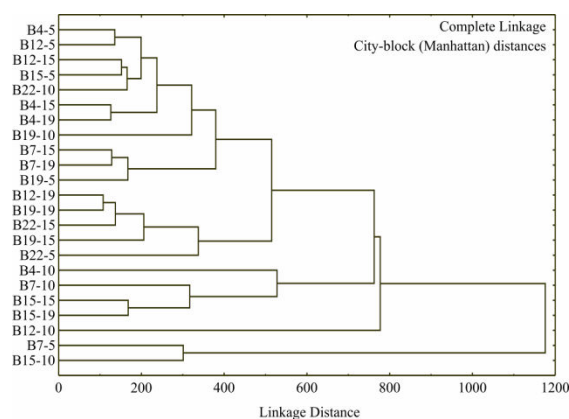


Fig. 4. Dendrogram of clustering of samples with respect to trace element content upon extraction.

According to the ‘city block’ illustrated in Fig. 4, the coal ash from the sampling points B4-5 and B12-5 are connected at linkage distance 140, which refers to the similarity in their chemical composition, i.e. content of 32 identified trace elements including REE. This linkage distance, i.e. 140, is identified for several other pairs of samples: B19-19 and B22-15, B4-15 and B4-19, B7-15 and B7-19. The sample pairs B12-15 and B15-5 are connected at 150 linkage distance. The same linkage distance is applicable for the following pairs: B15-15 and B15-19, B15-5 and B22-10, B7-19 and B19-5. B12-19 and B19-19 are connected at a smaller linkage distance, i.e. 100. Samples B7-5 and B15-10, as well as B7-10 and B15-19 are connected at 300 linkage distance. The linkage distance of 200 is characteristic for B22-15 and B19-15, and B12-5 and B15-5, while B12-15 and B4-19 are associated at slightly higher length (220 linkage distance). Several samples are connected at linkage distances above 300. Namely, B15-5 and B19-9 are connected at 320, B22-15 and B22-5 at 370, and B4-15 and B7-19 at 380. Linkage distances for following pairs are even higher: B4-10 and B15-15 are connected at 560, as well as B19-10 and B19-5. B12-19 and B7-10 are connected at 760 linkage distance, and B19-15 and B12-10 at 770. B7-10 and B7-5 is connected at 1190.

According to the dendrogram there are similarities between multiple samples grouped in the clusters. There are smaller cluster such as B4-19, B19-9, B7-15 and B7-19 group, and another group that comprises B12-5, B15-5, B22-10 and B4-15. Also the cluster with B15-15, B15-19, B12-10 and B7-5 can be characterized as smaller. However, there are three huge clusters. The first big cluster merges the following samples together: B12-19, B19-19, B22-15, B19-15, B22-15, B4-10, and B7-10. The second big cluster comprises B7-15, B7-19, B19-5, B12-19, B19-19, B22-15, and B19-15, and finally the third big cluster contains B22-5, B4-10, B7-10, B15-15, B15-19, and B12-10.

The disposition of 32 trace elements, including REE, and 24 coal ash samples are illustrated in the PCA diagram (Fig. 5).

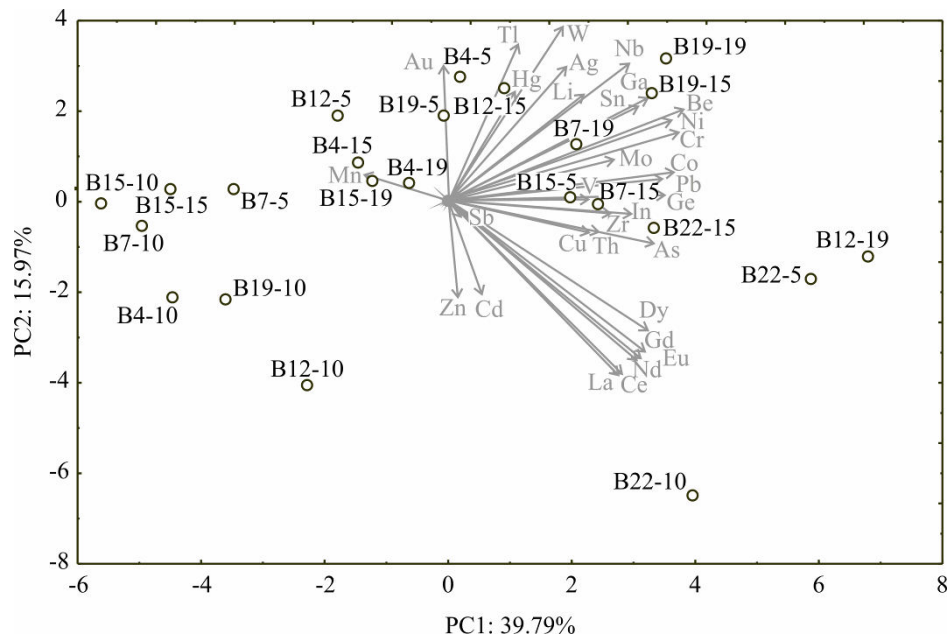


Fig. 5. PCA graph of the variables based on component correlations.

The points shown in the PCA graph, which are geometrically close to each other, indicate the similarity of the patterns that represent these points. The orientation of the vector describing the variable in the factor space indicates an increasing trend of these variables. The

length of the vector is proportional to the square of the correlation values between the fitting value for the variable and the variable itself. The angles between corresponding variables indicate the degree of their correlations (small angles corresponding to high correlations).

The PCA of the presented data explained that the first two components accounted for 56.44 % of the total variance (41.39 and 15.06 %, respectively) in the 32-variables system (trace elements). Considering the map of the PCA performed on the data, the contents of Co (which contributed 5.6 % of total variance, based on correlations), Ge (5.0 %), Pb (4.9 %), Cr (5.6%), Be (6.0 %) and Ni (5.4 %) exhibited the most intensive positive scores according to first principal component. The positive contribution to the second principal component calculation was observed for the content of: Au (5.3 % of total variance, based on correlations), Tl (7.0 %) and W (7.5 %), while negative scores on second principal component calculation were observed for the content of: Dy (13.6 %), Gd (7.7 %), Eu (8.0 %), Nd (8.3 %), La (10.2 %), and Ce (9.9 %). As expected the identified REE were grouped and their content was relatively low in comparison to other trace elements.

As it can be seen from the PCA graph in Fig. 5, Mn is singled out and positioned at the left side of the diagram, since its quantity was among the highest. Very high quantity of Mn was characteristic for the samples: B4-10, B4-15, B4-19, B12-10, B12-5, B19-5, B19-10, B15-19, B15-10, B15-15, B7-5 and B7-10. Relatively high amounts of Zn and Cd, which are situated at the lower half of the diagram, are characteristic for the following samples: B4-10, B19-10, B12-10, B22-5, B12-19, and B22-10. The majority of the trace elements (Tl, Au, W, Hg, Nb, Ag, Li, Ga, Sn, Be, Ni, Cr, Mo, V, Co, Pb, Ge, In, Sb, Zr, Cu, Th, and As) are positioned at the upper right side of the PCA graph together with the samples: B4-5, B12-15, B15-5, B7-15, B22-15, B7-19, B19-19, B19-15, B22-15, B12-19, B19-5, and B22-5. The high concentration of Au can be found in the B19-5 and B4-5 samples. Tl, W, Hg, and Ag are characteristic for the B12-15 sample, while Li and Nb can be found in B19-19. Samples B7-19 and B19-15 are characterized by high concentrations of Sn, Be, Ni, Cr, and Ga. B15-5 and B7-15 are abundant in Mo, V, Co, Pb, and Ge, while B22-15, B12-19, B22-5 have high concentration of Cu, Th, Zr, In, and As. REE (Dy, Gd, Eu, Nd, Ce, and La) are separated and positioned at the lower right corner of the diagram. According to the principal component analysis, REE were especially high on the B22 sampling position on TENT-A landfill, i.e. in the coal ash samples B22-5, B22-10, and B22-15 upon five stage extraction.

4. Conclusion

An environmentally benign and economically sustainable procedure for the isolation of rare earth elements from the unconventional resource, i.e. an industrial byproduct, was developed. Upon analyzing twenty-four coal combustion ash samples from the different positions and various depths of the TENT-A thermal plant's landfill and conducted a five-stage extraction procedure, the total of thirty-two trace elements were successfully isolated. Six of the extracted elements, i.e. La, Ce, Ng, Eu, Gg, and Dy, belong to the rare earth elements (REE) group. The extraction can be considered successful only if all five stages are conducted. Acquired mean values (in mg/kg) of REE were: 0.18 (La), 0.39 (Ce), 0.33 (Nd), 0.02 (Eu), 0.08 (Gd), and 0.10 (Dy).

The spatial disposition of REE varied throughout the landfill. The B22 sampling position was characterized with the highest REE content. Ce, Eu, Dy, and La concentrations increased with the depth of the sampling borehole, while the concentrations of Nd and Gd did not significantly vary with respect to the depth and sampling disposition. There are strong correlations with REE and other trace elements. Namely, Nd, Eu, Gd, and Dy are strongly correlated to As, Pb and Ge; La with Ge; and Ce with As. Dysprosium had the most abundant correlations with REE and the rest of trace elements (As, Cr, Co, Ni, Pb, Zn, Ge, and In).

Despite relatively low amounts of REE and necessity of all five stages of extraction, this procedure can be considered sustainable because used the raw material is economical as it is an industrial byproduct. REE obtained from the five stage extraction from coal combustion ash can improve domestic supplies of these critical materials.

Acknowledgments

This investigation is financially supported by Ministry of Education, Science and Technological Development of the Republic of Serbia (contract no.: 451-03-68/2020-14/200012

5. References

1. Ecoba: <http://www.ecoba.com/ecobaccputil.html>
2. M. Izquierdo, X. Querol, *Int J Coal Geol* 94 (2012) 54.
3. N. Kockal, T. Ozturan, *J. Hazard Mater* 179 (2010) 954.
4. M. Alouani, S. Alehyen, M. Achouri, M. Taibi, *Chem Data Collect* 23 (2019) <https://doi.org/10.1016/j.cdc.2019.100265>
5. B. Pourrut, A. Lopareva-Pohu, C. Pruvot, G. Garçon, A. Verdin, C. Waterlot, G. Bidar, P. Shirali, F. Douay, *Sci Total Environ* 409 (2011) 4504.
6. I. Sýkorová, M. Havelcová, A. Zeman, H. Trejtnarová, *Sci. Total Environ* 409 (2011) 4606.
7. Y. He, Q. Luo, H. Hu, *Procedia Environ Sci* 16 (2012) 690.
8. K. Fujii, K. Ochi, A. Ohbuchi, Y. Koike, *J Environ Manage* 217 (2018) 157.
9. Z. Yu, C. Ni, M. Tang, X. Shen, *Const Build Mater* 175 (2018) 458.
10. Z. Wei, B. Wang, G. Falzone, E. Plante, G. Sant, *J CO₂ Util* 23 (2018) 117.
11. E. Tkaczewska, *Constr Build Mater* 70 (2014) 388.
12. J. Bijeljić, N. Ristić, Z. Grdić, D. Đorđević et al, *Sci Sint* 52 (2020) 231.
13. M. Hadi, M. Al-Azzawi, T. Yu, *Constr Build Mater* 175 (2018) 41.
14. S. Nedunuri, S. Sertse, S. Muhammad, *Constr Build Mater* 238 (2020) <https://doi.org/10.1016/j.conbuildmat.2019.117561>
15. Y. Hefni, Y. El Zaher, M. Waha, *Constr Build Mater* 172 (2018) 728.
16. F. Jiang, L. Zhang, E. Mukiza, Z. Qi., D. Cang, *J Alloy Compd* 749 (2018) 750.
17. V. Karayannis, A. Moutsatsou, A. Domopoulou, et al., *J Build Eng* 14 (2017) 1.
18. A. Mohammadinia, A. Arulrajah, S. Horpibulsuk, A. Chinkulkijniwat, *J Hazard Mater* 321 (2017) 547.
19. T. Almahayni, N. Vanhoudt, *J Hazard Mater* 349(2018) 128.
20. C. Lanzerstorfer, *Fuel* 228 (2018) 263.
21. P. Brown, T. Jones, K. Bérubé, *Environ Pollut* 159 (2011) 3324.
22. C. Belviso, F. Cavalcante, S. Di Gennaro, A. Palma, P. Ragone, S. Fiore, *Fuel* 144 (2015) 369.
23. U. Sharma, N.Gupta, K. Saxena, *Materials Today: Proceedings* (2020) <https://doi.org/10.1016/j.matpr.2020.06.211>
24. B. Kutchko, A. Kim, *Fuel* 85 (2006) 2537.
25. S. Shaheen, P. Hooda, C. Tsadilas, *J Environ Manage* 145 (2014) 249.
26. N. Gupta, V. Gedam, C. Moghe, P.Labhasetwar, *Environ Technol Innovation* 16 (2019) <https://doi.org/10.1016/j.eti.2019.100461>.
27. P. Asokan, M. Saxena, S. Asolekar, *Resour Conserv Recycl* 43 (2005) 239.
28. M. Gray, K. Champagne, Y. Soong, R. Killmeyer, et al., *Fuel Process Technol* 76 (2002) 11.

29. Y. Soong, M. Schoffstall, M. Gray, J. Knoer, K. Champagne, R. Jones R., Sep Purif Technol 26 (2002) 177.
30. H. Ban, T. Li, J. Hower, J. Schaefer, J. Stencil, Fuel 76 (1997) 801.
31. A. Meawad, D. Bojinova, Y. Pelovski, Waste Manag 30 (2010) 2548.
32. A. Kolker, C. Scott, J. Hower, J. Vazquez, C. Lopano, S. Daie, Int J Coal Geol 184 (2017) 1.
33. Z. Huang, M. Fan, H. Tiand, J Rare Earth 36 (2018) 337.
34. B. Li, Y. Wei, N. Li, T. Zhang, J. Wang, Sci Sint 52 (2020) 195.
35. A. Hamza, F. Benabdallah, I. Kallel, L. Seveyrat, H. Khemakhem, J Alloy Compd 735 (2018) 2523.
36. X. Fei Zhang, X. Xie, Q. Xu, M. Chen, D. Chu Chen, D. Ping Huang, F. Zhang, Science of Sintering, 51 (2019) 295.
37. G. Singh Kathait, M. K. Panda, N. S. Panwar, Sci Sint 52 (2020) 97.
38. A. Smoliński, M. Stempin, N. Howaniec, Spectrochim Acta Part B 116 (2016) 63.
39. L. Chen, Y. Wu, H. Dong, M. Meng, J. Chen, Sep Purif Technol 197 (2018) 70.
40. H. Yuan, W. Hong, Y. Zhou, B. Pu, Y. Liu, J Rare Earth 36 (2018) 642.
41. D. Qi, Rare Earth – Chapter 2 (2018): 187.
42. Y. Wang X. Su, H. Zhou, X. Sun, Hydrometallurgy, 179 (2018) 181.
43. A. Seidel, Y. Zimmels Chem. Eng. Sci. 1998; 53: 3835-3852.
44. H. Abdi, L. Williams, Principal component analysis, Wiley Interdisciplinary Reviews. Comp. Stat. 2 (2010) 433.

Сажетак: Елементи који припадају групи ретких земаља (REE) представљају основу за многа унапређења у модерној индустрији с обзиром да имају широк спектар примене првенствено због својих електро-магнетских и оптичких својстава. Елементи из групе ретких земаља се примењују у производњи катализатора, магнета и као допант у за различите керамичке материјале. Минерали који садрже ретке земаље су изузетно слабо заступљени у природи, због чега се непрекидно истражују нови неконвенционални ресурси који садрже ове елементе - попут отпадних материјала и индустријских нуспроизвода. Продукти сагоревања угља садрже концентрације ретко земних елемената у распону између 200 до 1500 ppm. Ова се количина REE се може изоловати поступком екстракције. У овом истраживању спроведена је петостепенa екстракција REE из пепела добијеног сагоревањем угља и одложеног на депонију термо-електане ТЕНТ-А. Извршена је екстракција 32 елемента (As, Ga, Ce, Be, Ge, Nd, Cr, Zr, Eu, Cu, Nb, Gd, Co, Mo, Dy, Li, Ag, W, Mn, Cd, Au, Ni, U, Hg, Pb, Sn, Tl, V, Sb, Th, Zn, La). Хемијске анализе урађене су помоћу XRF, ICP-OES, ICP-MS и AAS техника. Сложеност добијених података испитана је анализом главних компонената (PCA) и кластер анализом (CA) како би се утврдиле међусобне везе, количине елемената и карактеристике одлагалишта, као и међусобни односи елемената који су од интереса. На овај начин је урађена процена могућности добијања елемената из групе ретких земаља из угљеног пепела.

Кључне речи: ситнозрни материјали; индустријски нуспроизводи; хемијска екстракција; аналитичко моделовање; допанти за керамичке материјале.

